Beta-limiting Instabilities and Global Mode Stabilization in NSTX*

S. A. Sabbagh,[1†] R. E. Bell,[2] M. G. Bell,[2] J. Bialek,[1] A. H. Glasser,[3] B. LeBlanc,[2] J.E. Menard,[2] F. Paoletti,[1] D. Stutman,4 E. Fredrickson,[2] A. M. Garofalo,[1] D. Gates,[2] S. M. Kaye,[2] L. L. Lao,[5] R. Maingi,[6] D. Mueller,[2] G. Navratil,[1] M. Ono,[2] M. Peng,[6] E. Synakowski,[2] W. Zhu,[1] and the NSTX Research Team

[1] *Department of Applied Physics and Applied Mathematics, Columbia University, New York, New York*

[2] *Princeton Plasma Physics Laboratory, Princeton University, Princeton, New Jersey*

[3] *Los Alamos National Laboratory, Los Alamos, New Mexico*

[4] *Johns Hopkins University, Baltimore, Maryland*

[5] *General Atomics, San Diego, California*

[6] *Oak Ridge National Laboratory, Oak Ridge, Tennessee*

Research on the stability of spherical torus plasmas at and above the no-wall beta limit is being addressed on NSTX, which has produced low aspect ratio plasmas, R/a ~ 1.27 at plasma current exceeding 1.4 MA with high energy confinement (TauE/TauE_ITER89P > 2). Toroidal and normalized beta have exceeded 25%, and 4.3, respectively in q ~ 7 plasmas. The beta limit is observed to increase and then saturate with increasing l_i. The stability factor β_N/l_i has reached 6, limited by sudden beta collapses. Increased pressure peaking leads to a decrease in β_N. Ideal stability analysis of equilibria reconstructed with EFIT show that the plasmas are at the no-wall beta limit for the n = 1 kink / ballooning mode. Low aspect ratio and high edge q theoretically alter the plasma stability and mode structure compared to standard tokamak configurations. Below the no-wall limit, stability calculations show the perturbed radial field is maximized near the center column and mode stability is not highly affected by a nearby conducting wall due to the short poloidal wavelength in this region. In contrast, as beta reaches and exceeds the no-wall limit, the mode becomes strongly ballooning with long poloidal wavelength at large major radius and is highly wall stabilized. In this way, wall stabilization is more effective at higher beta in low aspect ratio geometry.

The resistive wall mode has been observed in plasmas exceeding the ideal no-wall beta limit and leads to rapid toroidal rotation damping across the plasma core.

[*]Supported by US DOE Contracts DE-FG02-99ER54524 and DE-AC02-76CH03073.
[†]Present address: Princeton Plasma Physics Laboratory, Princeton University, Princeton, N.J. 08543

I. INTRODUCTION

Plasma stability at high ratio of plasma energy to magnetic field energy is required for economically attractive operation of a thermonuclear fusion reactor based on magnetic confinement. A figure of merit typically used for tokamak devices is the toroidal beta, $\beta_t \equiv 2\mu_0 \langle p \rangle / B_0^2$, of the system where $\langle p \rangle$ is the volume-averaged plasma pressure, and B_0 is the vacuum toroidal field at the plasma geometric center. Development toward greater efficiency in advanced tokamak and spherical torus (ST) reactor designs[1] has defined additional criteria, including a large fraction of bootstrap current to minimize power requirements for auxiliary systems. Plasma current profiles in largely bootstrap driven equilibria are generally broad (have low plasma internal inductance, l_i). However, tokamak experiments have shown that low l_i plasmas yield reduced β_t limits caused by the destabilization of magnetohydrodynamic (MHD) instabilities.[2,3] This contradiction has motivated both theoretical[4,5] and experimental[6] investigation of the stabilization of low l_i plasmas. Advanced tokamak plasmas in DIII-D have been stabilized utilizing conducting structure (wall stabilization) and feedback systems at values of β_t significantly above the level possible without stabilizing systems.[7] In contrast, stabilization of the spherical torus using similar tools is not yet established. While the START[8] spherical torus was successful in reaching high β_t at plasma current, I_p, up to 0.3 MA, determination of beta-limiting instabilities and the characteristics of these modes in high current (I_p > 1 MA) ST plasmas remains to be investigated. Dependence of stability limits on equilibrium parameters for low aspect ratio plasmas has been examined theoretically.[9-11] Details of the instabilities and their stabilization such as mode structure and related coupling to conducting walls can be significantly different in an ST compared to the advanced tokamak, due to the low aspect ratio and relatively high edge safety factor.

Research in the National Spherical Torus Experiment[12] (NSTX) has been conducted to establish the stable high β_t operating space of an I_p > 1 MA device, to identify and study the instabilities that limit β_t, and to initiate wall-stabilized plasma experiments. The device has a

major radius, R_0 = 0.86 m, and a midplane half-width of 0.7 m. The plasma current has exceeded 1.4 MA, and the on-axis vacuum toroidal field, B_0, is typically produced in the range 0.3 - 0.45 T. Auxiliary heating and current drive systems include 5 MW of neutral beam injection (NBI) and 6 MW of high-harmonic fast wave (HHFW) power. Plasma elongation, κ, and triangularity, δ, have reached 2.5 and 0.7, respectively. Operation of limiter, and both double and single-null divertor configurations have been established.[13] To provide passive stabilization of gross plasma modes, the device has a set of stabilizing conducting copper plates, arranged as four segmented toroidal rings (FIG. 1). The plates are indirectly connected electrically through high resistance supports that mount the plates to the vacuum vessel. For diagnosis of MHD instabilities, the machine has both toroidal and poloidal arrays of magnetic pickup coils, horizontal and vertical fans of ultra soft X-ray detectors, and a set of six locked mode detectors that surround the device at the midplane. Toroidal rotation profiles are measured with 20 ms time resolution by a charge exchange recombination spectroscopy diagnostic.

Computed ideal MHD stability limits determined during the conceptual design of NSTX ranged from β_t ~ 25% without the aid of a conducting wall (no-wall β_t limit), to β_t exceeding 40% in wall stabilized configurations with optimized equilibrium profiles.[14,11] Recent experiments in the device have produced plasmas with β_t values reaching the no-wall limit as shown in FIG. 2 where β_t at maximum plasma stored energy as determined by NSTX EFIT reconstructions using external magnetics is plotted against the Troyon scaling parameter, I_p/aB_0, where a is the plasma minor radius. The instabilities that set the present β_t limit and the behavior of this limit as a function of equilibrium profiles are described in Section II. Stabilization of low toroidal mode number kink/ballooning instabilities are theoretically investigated in Section III. Here, we find that relative to the advanced tokamak, mode coupling to conducting structure is relatively weak until the instability becomes strongly ballooning. Section IV describes the initial experimental investigation of global mode coupling to passive conducting structure in the spherical torus, and the identification of the resistive wall mode in the device. A summary and discussion of accessing β_N beyond the no-wall ideal limit based on the present results is given in

Section V.

II. BETA LIMITING INSTABILITIES AND OPERATING SPACE

Several plasma instabilities identified in tokamak experiments have now been observed in NSTX. These results have enabled initial studies of the physical similarities and differences of these modes in ST magnetic field geometry. In this paper, two classes of beta-limiting modes in NSTX are studied - ideal low-n kink/ballooning modes and resistive wall modes. These instabilities lead to relatively fast and large reductions in plasma stored energy at large normalized beta, $\beta_N \equiv 10^8 < \beta_t > aB_0/I_p$, but rarely lead to a full current quench. Other beta limiting instabilities include neoclassical tearing modes (NTMs)[15], current-driven kinks,[16,17] and locked modes. NTMs lead to beta saturation, rather than fast beta collapses. Current-driven kinks have been studied in specific low edge safety factor, q_a, experiments and can typically be avoided in standard machine operation. Locked modes can be beta-limiting, but are typically eliminated through alteration of the plasma startup phase or gas puffing. Sawteeth with small inversion radii created by slowed minor radial growth during startup are observed and are benign except at sufficiently high poloidal beta when they can trigger NTMs. In general, however, operation with EFIT reconstructed central safety factor greater than unity is required to avoid strong toroidal mode number, $n = 1$ mode activity that typically precedes beta collapse.[13] Compressional Alfven eigenmodes have also been identified but are not observed to be beta-limiting.[18]

Elements of establishing the fundamental plasma operating space in NSTX including density limits,[16] flux consumption,[19] and MHD equilibrium parameters and configurations[13] have been reported. The present aim is to study instabilities limit β_t in NSTX. Once determined, plasma stability can be approached in two ways, (i) determine how beta limits vary with equilibrium profiles and boundary shape so that optimal parameters can be chosen to avoid instability, and (ii) examine how systems can be effectively applied to stabilize modes if instability cannot be avoided. The latter approach is important since in an actual experiment, optimizations are normally limited by practical considerations. Also, advanced tokamak research

has shown that significant increases in β_t can be realized for global MHD instabilities by conducting wall stabilization and active feedback once the no-wall β_t limit has been violated.[20,21] Recently, stabilization of NTMs has also been demonstrated,[22] with some experiments reaching maximum β_t after mode suppression.[23]

Experimentally, the maximum β_N increases with increasing current profile peaking in NSTX until l_i reaches 0.7, while at higher l_i, the maximum β_N saturates with increasing l_i (FIG. 3). The increase of β_N with l_i is well-known in advanced tokamak research and correlates with maintaining ideal MHD stability.[2,3] In DIII-D (Ref. 2), a reduction of β_N with increasing l_i at high values of l_i was reported due to the onset of internal instabilities. However, using specially tailored current profiles through negative plasma current ramping, this reduction can be avoided. Instead, a saturation of β_N at higher $l_i < 1.3$ is shown in FIG. 3. Another significant difference in NSTX is that a substantial portion of the present database has exceeded the DIII-D β_N limit of $4l_i$ with plasmas reaching $6l_i$. Fast beta collapses are observed at all values of l_i. Beta saturation coincident with NTM activity typically occurs in high current plasmas with poloidal beta greater than 0.4. A clear reduction of the maximum β_N with increasing pressure profile peaking, $F_{p\_mag} \equiv p_{mag}(0) / \langle p_{mag} \rangle$, where p_{mag} is the EFIT reconstructed (using external magnetics alone) total plasma pressure, is also observed (FIG. 4). The significant quantitive decrease of β_N with increasing F_{p_mag} illustrates the importance of reduced pressure peaking in attaining maximum β_N in NSTX. The figure illustrates that by increasing l_i at fixed F_{p_mag}, β_N can be increased, but even at increased l_i, a reduction in β_N with increasing F_{p_mag} is evident. Dependence of the experimental beta limit on plasma boundary shape is presently under investigation.[24]

Agreement between the experimentally observed β_N limit due to fast beta collapses and the theoretically computed ideal MHD stability to low toroidal mode number kink/ballooning modes can be tested using the time evolution of equilibrium reconstructions. Ideal MHD stability analysis of NSTX EFIT reconstructions using external magnetic measurements qualitatively reproduce the experimental behavior of the β_N limit shown in Section II. However, to obtain quantitative agreement, equilibrium reconstructions must be refined by also including at least

partial kinetic pressure profile information and diamagnetic loop measurement to allow more accurate determination of the pressure peaking factor, F_p and plasma stored energy, W_{tot}. It is found that F_p is typically 50% larger than $F_{p\ mag}$, and W_{tot} typically increases by about 10% in partial kinetic versus magnetics-only reconstructions. For example, the largest β_t shown in FIG. 2 is 24.8%, while partial kinetic reconstruction of the same discharge yields a maximum β_N = 26.9%. The plasmas are strongly paramagnetic, and remain so at maximum β_t with a toroidal field increase of 41% at the magnetic axis. Regardless of this increase in the local magnetic field, the local β at the magnetic axis is 48%. As in magnetics-only fits, a single set of EFIT constraints has been determined for partial kinetic reconstructions to model all plasmas. Adhering to this set without varying constraints for specific equilibria allows a quantitative stability evaluation of the time evolution of the plasma equilibria in a single discharge, as well as a direct comparison of the stability of plasmas with significantly different pressure peaking factors and beta limits. Such a comparison is shown in FIG. 5, in which time-evolved ideal, no-wall MHD stability is computed using the DCON[25] code for two plasmas exhibiting fast beta collapses. Stability calculations begin at t = 0.15s, and continue with increasing time resolution (down to 2 ms) as the fast beta collapse time is reached. The pressure peaking factor evolves slowly in both discharges, with F_p = 3.7 in the discharge shown in FIG. 5(a) at the time of the beta collapse, and F_p = 2.9 in the discharge shown in FIG. 5(b) at the analogous time. In the plasma with larger F_p, the experimental β_N limit is 2.6, while the computed n = 1 ideal kink/ballooning mode becomes unstable at β_N = 2.4. In the plasma with smaller F_p, the experimental β_N limit is 4.2 while the computed n = 1 ideal kink/ballooning mode becomes unstable at β_N = 4.1. In both cases, high-n ballooning modes become unstable shortly before the n = 1 kink. Stability to the Mercier criterion is violated either shortly before or after the n = 1 mode becomes unstable.

III. KINK/BALLOONING MODE STABILIZATION IN ST GEOMETRY

Stabilization of global kink/ballooning instabilities in tokamaks relies on the presence of

a conducting wall to either stabilize rapidly rotating plasma modes (mode frequency, $\Omega_m >> 1/\tau_w$) where τ_w is the resistive decay time of the wall, or to slow the growth of slowly rotating or stationary modes, $\Omega_m \sim 1/\tau_w$, such as the resistive wall mode (RWM) in plasmas rotating below the RWM critical rotation frequency, Ω_c. In order for either scenario to succeed, the mode structure must allow coupling of the perturbed field to the conducting wall. However, ST magnetic field geometry yields mode structures that are significantly different than advanced tokamak counterparts and at similar β_N, lead to relatively weak wall coupling. This is illustrated in FIG. 6 that compares the theoretically computed poloidal variation of the normal field perturbation, δB_r, at the plasma edge between NSTX and DIII-D plasmas of similar $\beta_N \sim 2.3$. The normalized equal-arc length poloidal angle, $\theta/2\pi$ equals 0 and 1 at the outboard midplane, $R_0 + a$, where R_0 is the major radius of the device, and 0.5 at the inboard midplane, $R_0 - a$. The mode in the NSTX case lacks coupling to outboard conducting structure due to the near zero amplitude in this region. Also, the short poloidal wavelength of the mode on the inboard side causes a rapid amplitude reduction of the perturbed field away from the plasma surface. In constrast, the mode in DIII-D has maximum amplitude and relatively long poloidal wavelength on the outboard side. These characteristics lead to stronger coupling of the DIII-D mode to outboard conducting structure. In order for the NSTX case to couple well, the underlying equilibrium must have sufficient pressure drive to produce a mode that is ballooning. The short connection length in ST geometry will insure that the mode will have long poloidal wavelength on the outboard side.

The lack of wall stabilization due to weak mode coupling to the wall in the low β_N ST plasma can be shown by comparing no-wall to with-wall ideal MHD stability calculations of the potential energy functional, δW, computed by DCON for the NSTX plasma used in the previous comparison. The variation of stability with β_N is examined by scaling the pressure profile self-similarly from the original equilibrium. The lower pressure peaking, $F_{p\_mag} = 2.4$ was used for this illustration as it leads to a higher no-wall β_N limit and a wider gap in β_N between the no-wall and with-wall β_N limits. The results are shown in FIG. 7, the solid and dashed curves representing the with-wall and no-wall configurations, respectively. These equilibria generally

require finite edge current density to allow reliable reconstruction of the entire discharge.[13] The edge current can drive localized, or peeling modes that are well-known to appear at $n*q_a$ slightly below integer values.[26] The δW is therefore computed at approximate minimum and maximum values by varying q_a and both solutions are shown. The localized / peeling mode is typically unstable down to zero β_N, however this mode is not observed to be disruptive in NSTX. The no-wall limit, as compared to the experimental onset of fast beta collapse in FIG. 5 is therefore defined as the β_N value at which the maximum computed value of δW becomes negative. The poloidal variation of δB_r for the localized / peeling mode at β_N below the no-wall limit is similar to that shown for the NSTX case in FIG. 6, and as expected, the conducting wall has no effect on the stability of this mode until the no-wall limit is reached due to the lack of mode coupling to the wall. However, as β_N increases past the no-wall limit, the mode structure becomes more ballooning and couples to the conducting plates, allowing the mode to be wall stabilized. In this way, wall stabilization becomes more effective as β_N is increased. The maximum value of δW is affected by the conducting wall at lower $\beta_N \sim 3.5$, and the wall allows an increase of the stable operating β_N from 5.5 to 6.5 until the with-wall limit is reached, set by internal mode instability. The range of wall stabilized β_N is dependent upon l_i and F_p, however this range increases in size at higher β_N in the ST since the increased pressure drive provides the ballooning character of the mode that leads to greater wall coupling.

One could imagine that stabilization of the short poloidal wavelength mode might be possible using close conducting structure at $R_0 - a$. To check this, a conformal wall is considered in the calculation of δW. However, a conformal wall with a 1 cm gap to the plasma surface is required stabilize the mode at all values of β_N (FIG. 8). Since relatively high resistance plasma facing components of greater than 1 cm thickness are typically used in actual devices, inner wall stabilization is impractical in the ST.

IV. MODE COUPLING TO CONDUCTING WALL AND RESISTIVE WALL MODES

The relatively weak mode coupling to conducting structure in the ST expected from theory has guided experiments in NSTX to investigate mode coupling and generation of the resistive wall mode. Inboard limited plasmas were created that minimized the gap between the plasma boundary and the primary stabilizing plates in the device (the plates closest to the midplane). Since the present control system in NSTX allows steady plasma elongation of about 2, the minimal plasma / plate gap is approximately 11 cm when the plasma / limiter gap at the midplane is 1 cm. In this configuration, plasmas with sufficient NBI power either developed NTMs leading to beta saturation, or fast beta collapses. A comparison of these two cases are shown in FIG. 9. In the latter case, the resistive wall mode (RWM) was observed on the locked mode detector while the plasma stored energy increased. Characteristics of the RWM observed in these experiments are similar to those found in tokamaks.[7] The mode was observed when the ideal $n = 1$ no-wall β_N limit was violated through high power NBI heating (4.6 MW). The mode was not observed in control experiments in which lower NBI power (1.7 MW) was used. Calculation of the stability and eigenmode evolution show that the RWM is observed when the computed eigenfunction couples to the conducting wall. This is shown in FIG. 10, where the evolution of ideal $n = 1$ stability is computed for equilibrium reconstructions of the experimental discharge. Before the ideal no-wall limit is violated and the RWM is observed (t = 0.18 s), the eigenfunction has relatively small amplitude on the outboard side, closest to the stabilizing plates. However, as the ideal no-wall limit is violated and the RWM is observed, the eigenfunction balloons and couples to the stabilizing plates. As expected from the analysis given in Section III, the wall stabilized range of β_N is small ($\Delta\beta_N = 0.2$) as the plasma rapidly becomes internal mode unstable. The margin in β_N over the no-wall limit, or enhancement factor, $E_w = \beta_N/\beta_N^{\text{no-wall}} = 1.08$. The growth rate of the RWM observed determined from the growth of the locked mode detector signal is 5 ms. This agrees well with VALEN[27] code calculation of the growth time of 4.6 ms for the computed n = 1 mode in the presence of a detailed 3D model of the NSTX stabilizing plates, vacuum vessel, and center stack. Computed image currents are

maximum in the primary passive plates (FIG. 11). Based on this calculation, the RWM persists for 3.5 τ_w before termination at the beta collapse.

Evidence from additional diagnostics support the identification of the resistive wall mode. In contrast to a rotating plasma mode, the RWM is nearly stationary in the lab frame.[28] RWM growth in the locked mode detector was observed while the plasma was rotating, eliminating the possibility that the mode was a locked tearing mode. No precursors were observed in the magnetic pickup coils before the onset of the RWM. In contrast, clear n = 2 and n = 3 rotating modes were detected by these coils in the comparison plasma in which beta saturation was observed (FIG. 12). Soft X-ray emission shows a mode structure resembling a global kink in RWM plasmas leading up to the beta collapse. No core or edge islands were clearly observed, and the termination resembled a kinking of the plasma core. In contrast, a radially symmetric reconnection event was observed leading to the termination of the comparison plasma. RWM plasmas also exhibit a unique, rapid rotation decrease across the entire plasma core (FIG. 13a). Rotation damping rates of -300 kHz/s were observed while the RWM was present. The rotation damping occurred in spite of maximum neutral beam momentum input in these plasmas. In contrast, the comparison plasma with an $n = 2$ mode showed a core toroidal rotation that increased monotonically in time (FIG. 13b). The pickup coils showed the $n = 2$ mode with a frequency decreasing from approximately 6 to 3 kHz (FIG. 12). This reduction in frequency was consistent with the observed toroidal rotation damping in the edge region. The observed rotation damping rate was -75 kHz/s, significantly less rapid than that observed during RWM activity. Computation of the radial mode structure showed that the mode amplitude was greatest in the plasma core, where the observed toroidal rotation damping was strongest. This is consistent with RWM theory which predicts that rotation damping should scale as the square of the perturbed field caused by the mode.

V. SUMMARY AND DISCUSSION

Low aspect ratio, spherical torus plasmas with $I_p < 1.4$ MA and reaching the ideal no-wall beta limit have been created ($\beta_t > 25\%$). Experimentally, the β_N limit increases, then saturates with increasing l_i (current profile peaking), and decreases with increasing pressure profile peaking. Ideal low-*n* stability of partial kinetic equilibrium reconstructions quantitatively agrees with the experimental β_N threshold for fast beta collapses in the device. Theory predicts generally weak coupling to conducting structure in the range of β_N and pressure peaking presently reached in the experiment. Strong coupling, and therefore strong stabilization occurs through ballooning of the mode, producing a mode with long poloidal wavelength on the outboard side of the device. Inner wall stabilization of global modes in spherical torus field geometry is ineffective. Dedicated experiments have produced adequate wall coupling in a fairly narrow region of β_N space, and the resistive wall mode has been observed when the ideal no-wall limit was exceeded.

The present experimentation and analysis suggests specific routes to further increase β_N and β_t in NSTX. Operation with a broad pressure profile will lead to an increase of the no-wall beta limit, allowing stable access to increased β_N without wall stabilization. Sufficiently high $l_i \sim 0.7$ will be required to stabilize global modes under these conditions (greater than $l_i \sim 3.5$ envisioned for optimized equilibrium targets). With β_N sufficiently large, the increased pressure drive will cause global modes to balloon and create long poloidal wavelength modes on the outboard side of the device. These modes can then be effectively wall stabilized, and l_i can be reduced through RF current drive, or more naturally by the increasing bootstrap current that will occur as β_N and β_t continue to increase. Alternatively, the plasma could be run at high l_i without the aid of wall stabilization. However, this strategy is expected to yield a lower β_N limit and would be prone to internal mode instability unless the central safety factor is maintained above unity.

ACKNOWLEDGEMENTS

The first author would like to acknowledge enlightening discussions with Dr. Allen Boozer and Dr. Alan Turnbull regarding the interaction of marginally stable MHD modes and error fields. This research was supported by the U.S. Department of Energy under contracts DE-FG02-99ER54524 and DE-AC02-76CH03073.

[1] R.D. Stambaugh, V.S. CHAN, R.L. MILLER, *et al., Fusion Technology* **33** (1998) 1.
[2] Howl, A.D. Turnbull, *et al.*, *Phys. Fluids B* (1992).
[3] S.A. Sabbagh, R. A. Gross, M. E. Mauel, *et al., Phys. Fluids B* **3**, 2277 (1991).
[4] A.D. Turnbull, *et al.*, Phys. Rev. Lett. **74**, 718 (1995).
[5] C. Kessel, *et al.*, Phys. Rev. Lett. **72**, 1212 (1994).
[6] E.J. Strait, T.S. Taylor, A.D. Turnbull, *et al.*, Phys. Rev. Lett. **74**, 2483 (1994).
[7] A. Garofalo, A.D. Turnbull, E.J. Strait, *et al.*, Phys. Plasmas **6**, 1893 (1999).
[8] A. Sykes, *et al.*, Plasma Phys. Contr. Nucl. Fus. Res. **1**, 799 (1995).
[9] Y.-K.M. Peng and D.J. Strickler, Nucl. Fusion **26**, 769 (1986).
[10] S.A. Sabbagh, M.H. Hughes, M.W. Phillips, *et al.*, *Nuclear Fusion* **29** (1989) 423.
[11] J.E. Menard, S.C. Jardin, S.M. Kaye, *et al.*, Nucl. Fusion **37** 595 (1997).
[12] M. Ono, *et al.*, Nucl. Fusion **40**, 557 (2000).
[13] S.A. Sabbagh, S.M. Kaye, J.E. Menard, *et al.*, to appear in Nucl. Fusion **41**, # 11 (2001).
[14] F. Paoletti, S.A. Sabbagh, D. Gates, *et al.*, to be published in Nucl. Fusion (2002).
[15] D. Gates, *et al.*, Bull. Am. Phys. Soc. **46**, 138 (2001).
[16] S.M. Kaye, *et al.*, Phys. Plasmas, (2000).
[17] J. Manickam, *et al.*, Bull. Am. Phys. Soc. **46**, 260 (2001).
[18] E. Fredrickson, *et al.*, Phys. Rev. Lett.; APS DPP meeting 2001 invited talk, Bull. Am. Phys. Soc. **46**, 207 (2001) submitted to Phys. Plasmas.
[19] J.E. Menard, B.P. LeBlanc, S.A. Sabbagh, *et al.*, Nucl. Fusion **41**, 1197 (2001).
[20] A.M. Garofalo, A.D. Turnbull, M.E. Austin, *et al.*, Phys. Rev. Lett. **82**, 3811 (1999).
[21] A.M. Garofalo, APS DPP meeting 2001 invited talk, Bull. Am. Phys. Soc. **46**, 20 (2001) submitted to Phys. Plasmas.
[22] H. Zohm, *et al.*, IAEA 2000.
[23] R.J. LaHaye, *et al.*, APS DPP meeting 2001 invited talk, Bull. Am. Phys. Soc. **46**, 21 (2001) submitted to Phys. Plasmas.
[24] J.E. Menard and the NSTX Team, Bull. Am. Phys. Soc. **46**, 138 (2001).
[25] A.H. Glasser and M.S. Chance, Bull. Am. Phys. Soc. **42**, 1848 (1997).
[26] J. Manickam, Phys. Fluids B **4**, 1901 (1992).
[27] J. Bialek, A. Boozer, M.E. Mauel, G.A Navratil, Bull Am. Phys. Soc. **43**, 1831 (1998).
[28] A. Bondeson and D. J. Ward, Phys. Rev. Lett. **72**, 2709 (1994).

Figure Captions

FIG. 1. NSTX device cross-section. The position of the stabilizing plates and locked mode detector are shown.

FIG. 2. Toroidal beta vs. Troyon scaling parameter I/aB_0 for NSTX plasmas at maximum plasma stored energy.

FIG. 3. Maximum normalized beta vs. plasma internal inductance. β_N / l_i has significantly exceeded the well-known DIII-D scaling of 4, reaching a maximum value of 6 at $l_i \sim 0.7$.

FIG. 4. Maximum normalized beta vs. pressure peaking factor. β_N decreases with increasing pressure peaking. Plasmas indicated by solid points reach higher β_N at fixed F_p via current profile tailoring (increased l_i).

FIG. 5. Time evolution and computed ideal no-wall stability for discharges with different pressure peaking. At the time of the fast beta collapse, $F_p = 3.7$ for the discharge in frame (a), and $F_p = 2.9$ for the plasma in frame (b). The corresponding experimental β_N limits of 2.7 and 4.2 respectively are in quantitative agreement with the computed $n = 1$ ideal no-wall β_N limit for these plasmas. Stability calculations are performed from t = 0.15s in each discharge up to the time of the beta collapse.

FIG. 6. Comparison of the computed poloidal variation of the $n = 1$ radial field perturbation in NSTX and DIII-D plasmas at similar β_N. ST field geometry leads to a perturbation with relatively weak wall coupling.

FIG. 7. Effect of stabilizing wall on ST equilibria. The potential energy functional δW vs. β_N is shown for configurations including an approximation of the NSTX conducting wall (solid line) and with no wall (dashed line) for an extrapolation of an NSTX plasma to high β_N with a pressure peaking factor of 2.4. The δW is not significantly different between no-wall and with-wall configurations until the no-wall β_N limit is approached.

FIG. 8. Effect of various conducting walls on modes lacking ballooning structure in the ST. Curves are shown for conformal walls with 1, 2, and 5 cm gap, the NSTX wall, and no wall for comparison.

FIG. 9. Time evolution of plasma current, normalized beta, $n = 1$ radial field perturbation from the plasma, and pressure peaking factor for a plasma exhibiting a resistive wall mode leading to a fast beta collapse, and a comparable plasma without the RWM leading to a saturation in beta. The latter case has lower pressure peaking.

FIG. 10. Time evolution of computed δW and poloidal variation of δB_r for n = 1 instability in a plasma developing a RWM. The computation is performed including an

approximation of the NSTX wall (solid line) and with no wall (dashed line). The δB_r is shown at t = 0.18s (weak, but finite perturbation on the outboard side) and t = 0.192s (strong perturbation on the outboard side).

FIG. 11. VALEN calculation of image currents generated in NSTX conducting structure. Thicker arrows indicate regions of larger current.

FIG. 12. Mode frequency and toroidal mode number from toroidal pickup coil array for plasma exhibiting the RWM (frame (a)) compared to a plasma with rotating n = 2 and n = 3 modes (frame (b)). The RWM plasma shows no strong modes up to the fast beta collapse.

FIG. 13. Time evolution of toroidal rotation profiles in plasma exhibiting a RWM (frame (a)) compared to a plasma with an n = 2 rotating mode (frame (b)).

FIG. 14. Routes to high β_N operation in NSTX suggested by analysis of conducting wall mode stabilization in ST magnetic geometry.

FIG. 1

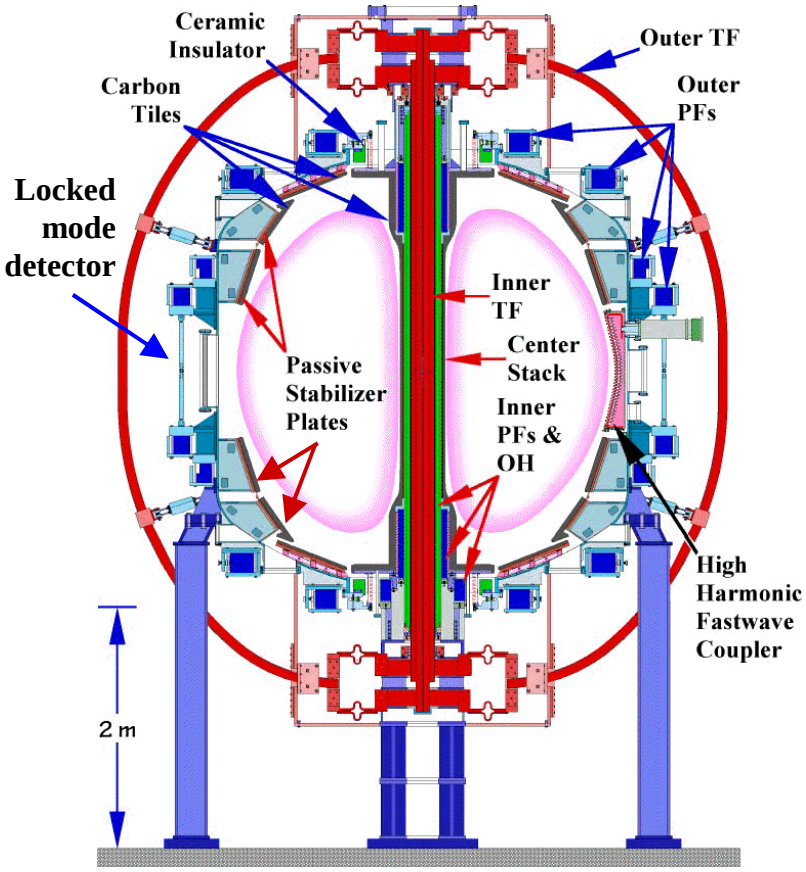
Ceramic Insulator
Carbon Tiles
Outer TF
Outer PFs
Locked mode detector
Inner TF
Center Stack
Passive Stabilizer Plates
Inner PFs & OH
High Harmonic Fastwave Coupler
2 m

FIG. 2

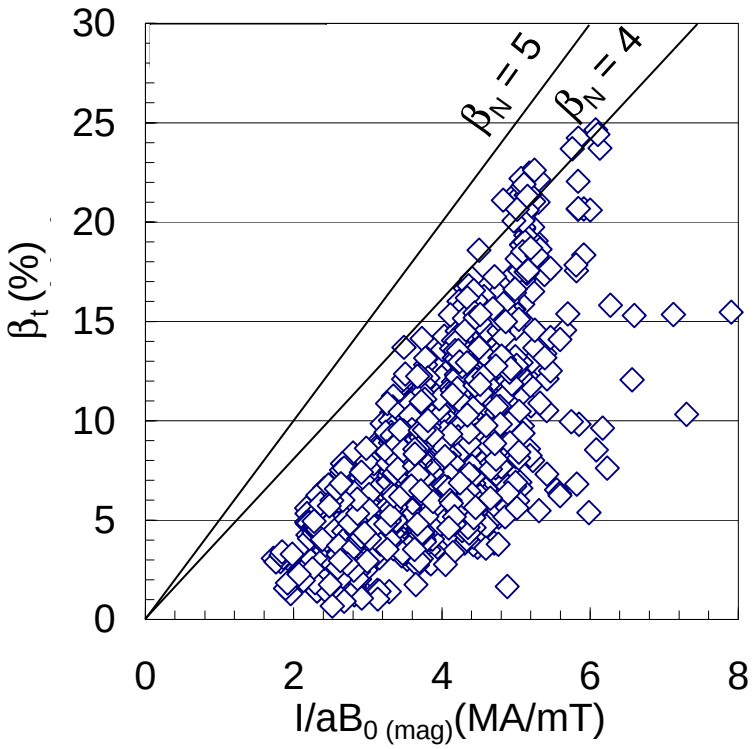

FIG 3.

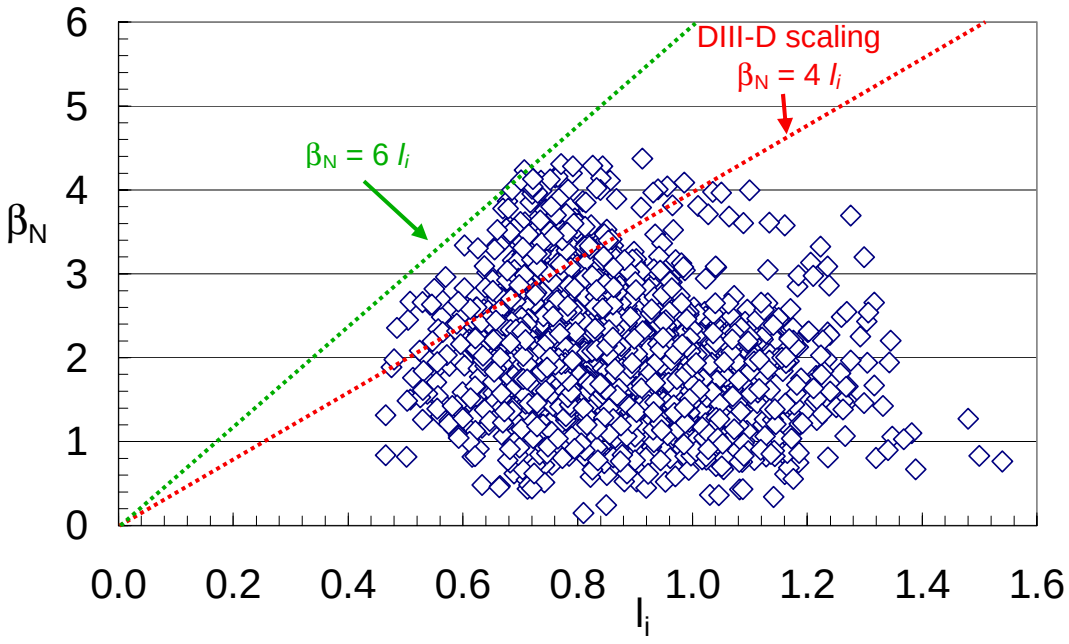
DIII-D scaling
$\beta_N = 4\, l_i$
$\beta_N = 6\, l_i$
β_N
l_i
0
1
2
3
4
5
6
0.0
0.2
0.4
0.6
0.8
1.0
1.2
1.4
1.6

FIG 4.

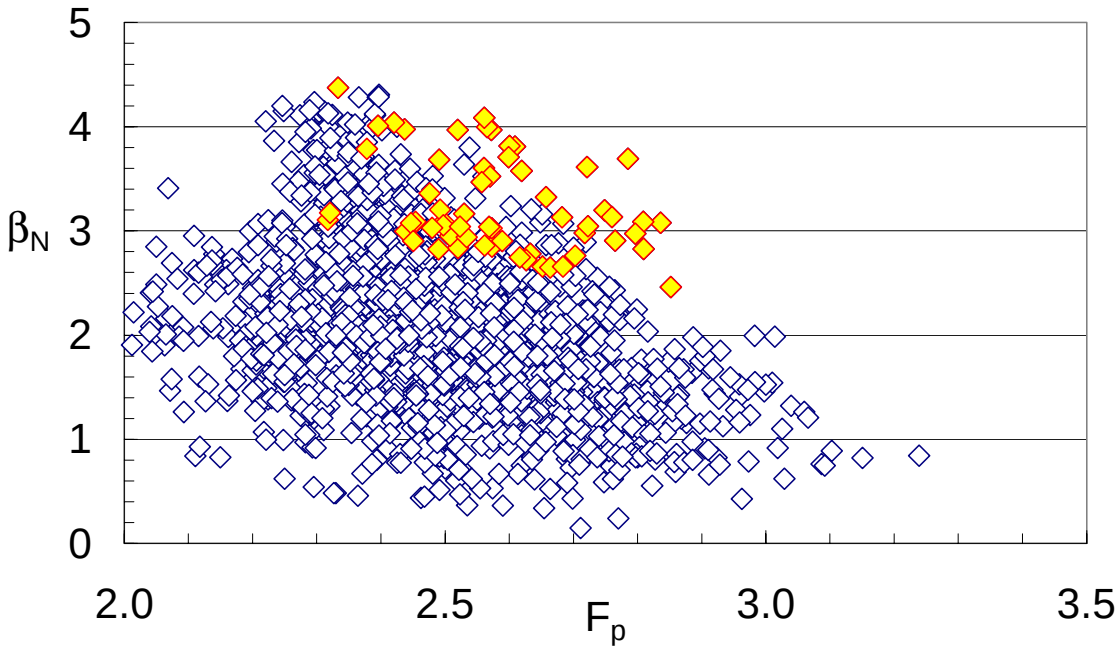
β_N
F_p
0
1
2
3
4
5
2.0
2.5
3.0
3.5

FIG 5.

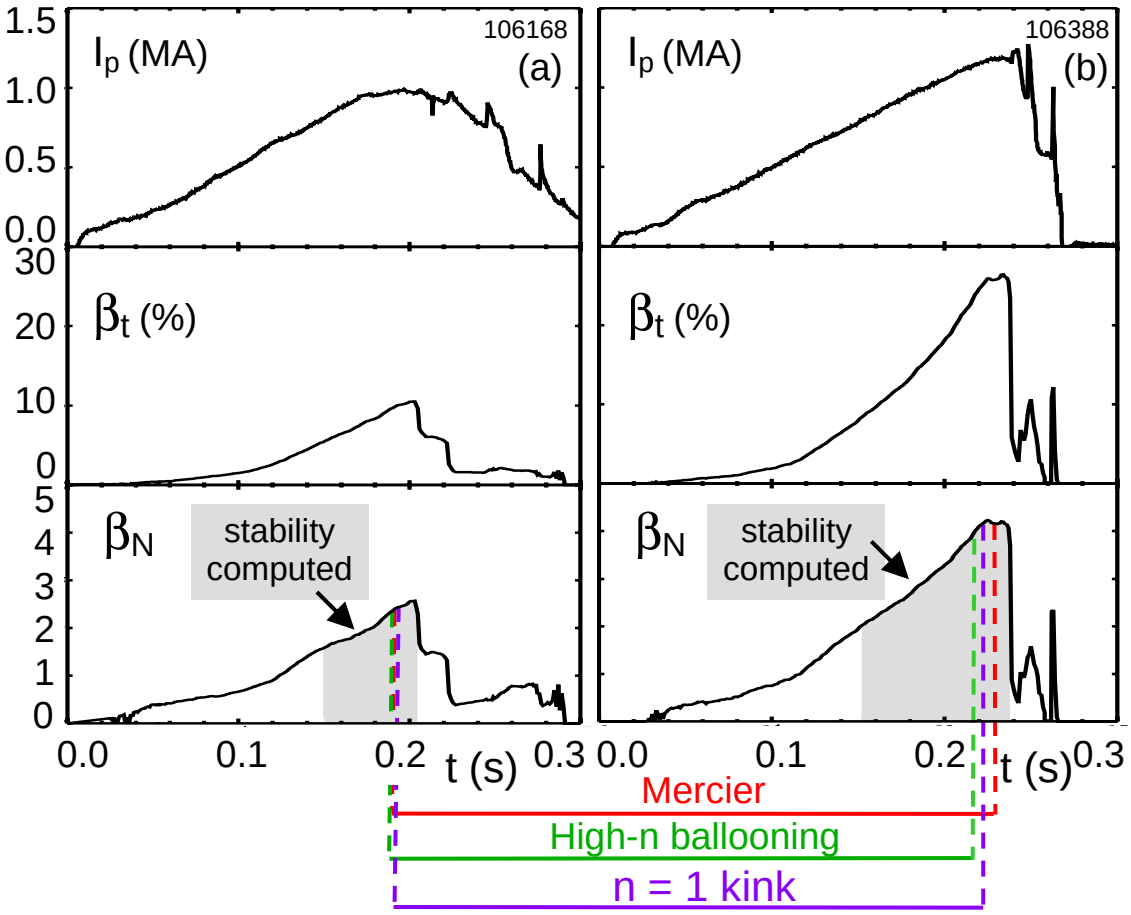
106168
(a)
I_p (MA)
1.5
1.0
0.5
0.0
β_t (%)
30
20
10
0
β_N
stability computed
5
4
3
2
1
0
0.0
0.1
0.2
0.3
t (s)
106388
(b)
I_p (MA)
β_t (%)
β_N
stability computed
0.0
0.1
0.2
0.3
t (s)
Mercier
High-n ballooning
n = 1 kink

FIG 6.

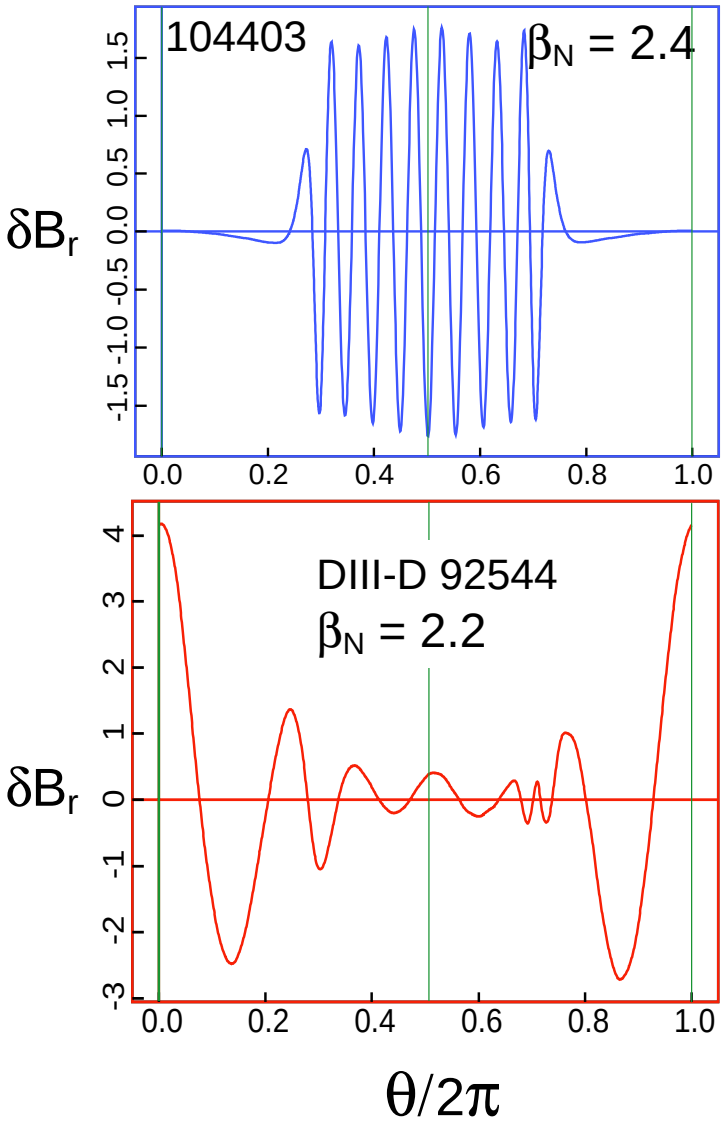
104403
β_N = 2.4
δB_r
1.5
1.0
0.5
0.0
-0.5
-1.0
-1.5
0.0
0.2
0.4
0.6
0.8
1.0
DIII-D 92544
β_N = 2.2
δB_r
4
3
2
1
0
-1
-2
-3
0.0
0.2
0.4
0.6
0.8
1.0
$\theta/2\pi$

FIG 7.

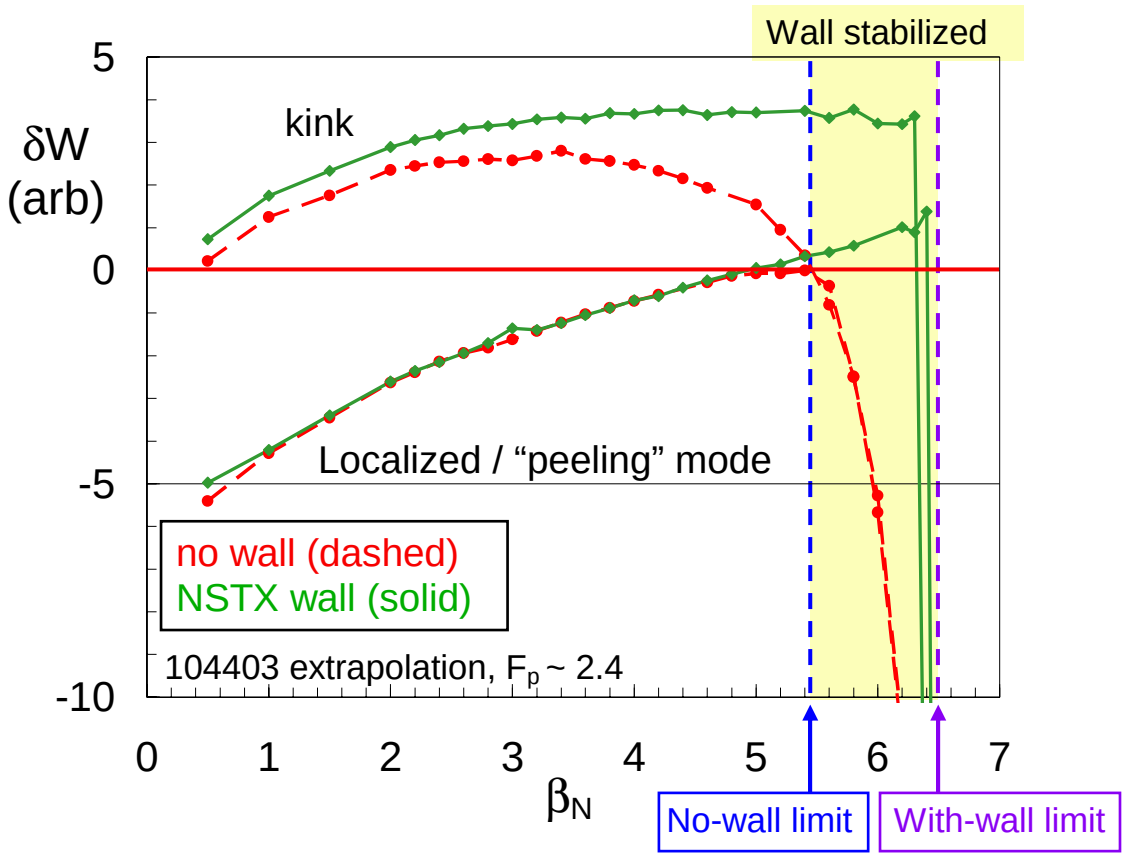
Wall stabilized
5
δW
(arb)
0
-5
-10
kink
Localized / “peeling” mode
no wall (dashed)
NSTX wall (solid)
104403 extrapolation, F_p ~ 2.4
0
1
2
3
4
5
6
7
β_N
No-wall limit
With-wall limit

FIG 8.

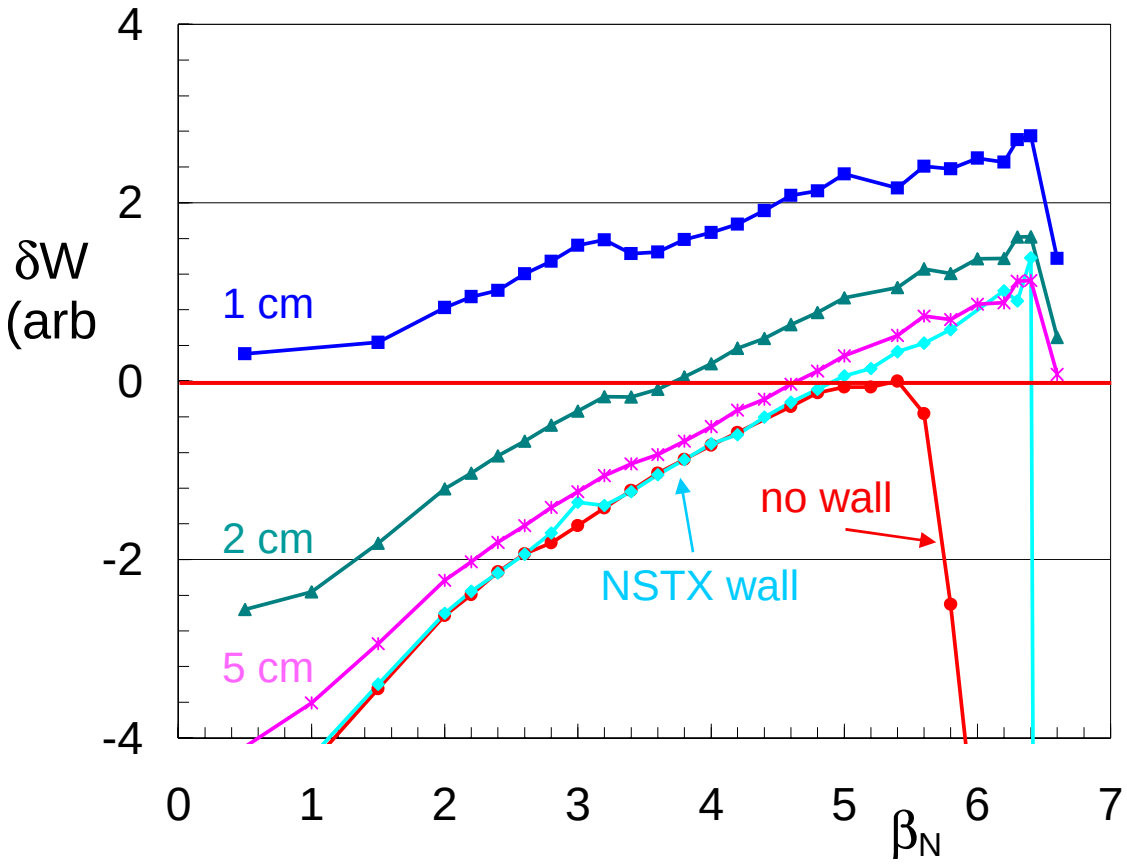

FIG 9.

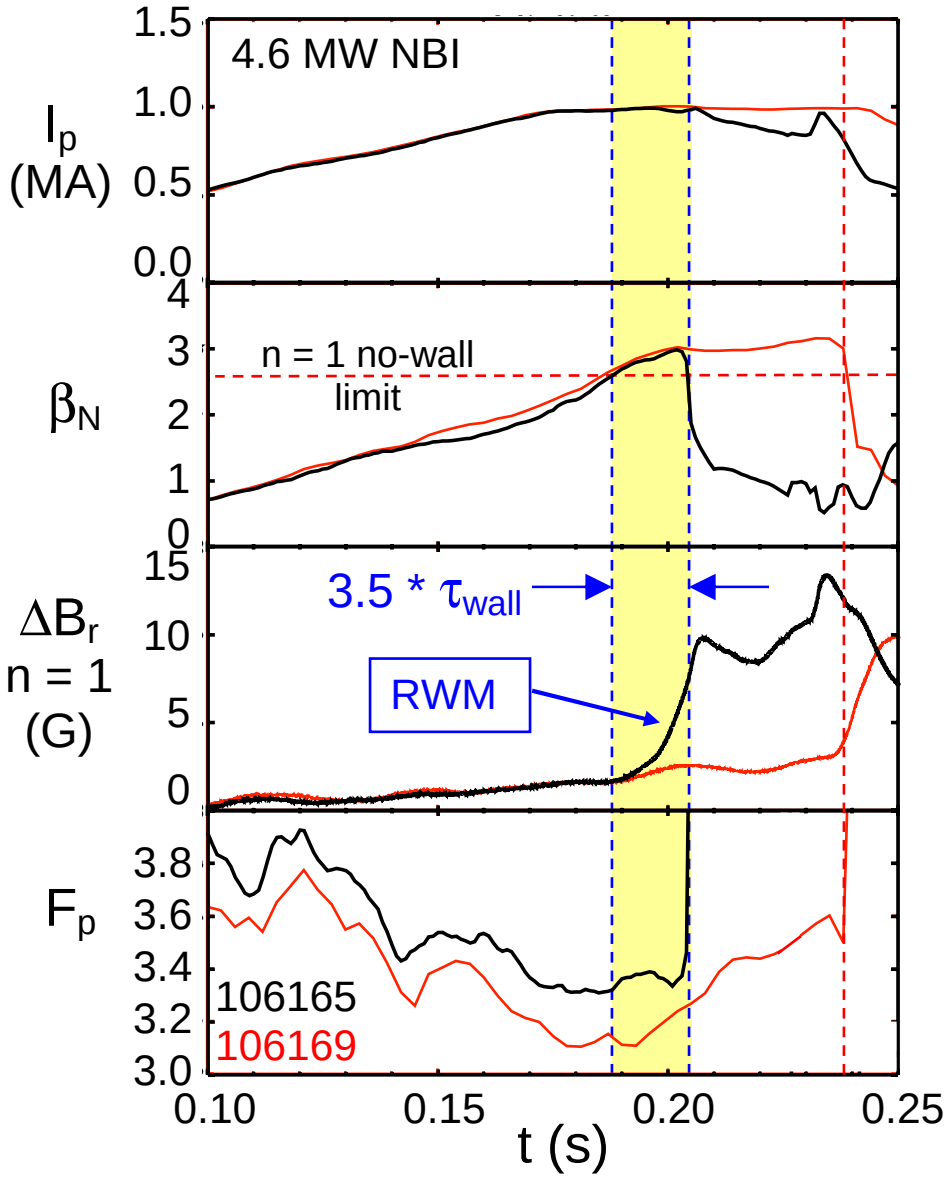
4.6 MW NBI
I_p (MA)
1.5
1.0
0.5
0.0
β_N
n = 1 no-wall limit
4
3
2
1
0
ΔB_r n = 1 (G)
3.5 * τ_{wall}
RWM
15
10
5
0
F_p
106165
106169
3.8
3.6
3.4
3.2
3.0
0.10
0.15
0.20
0.25
t (s)

FIG 10.

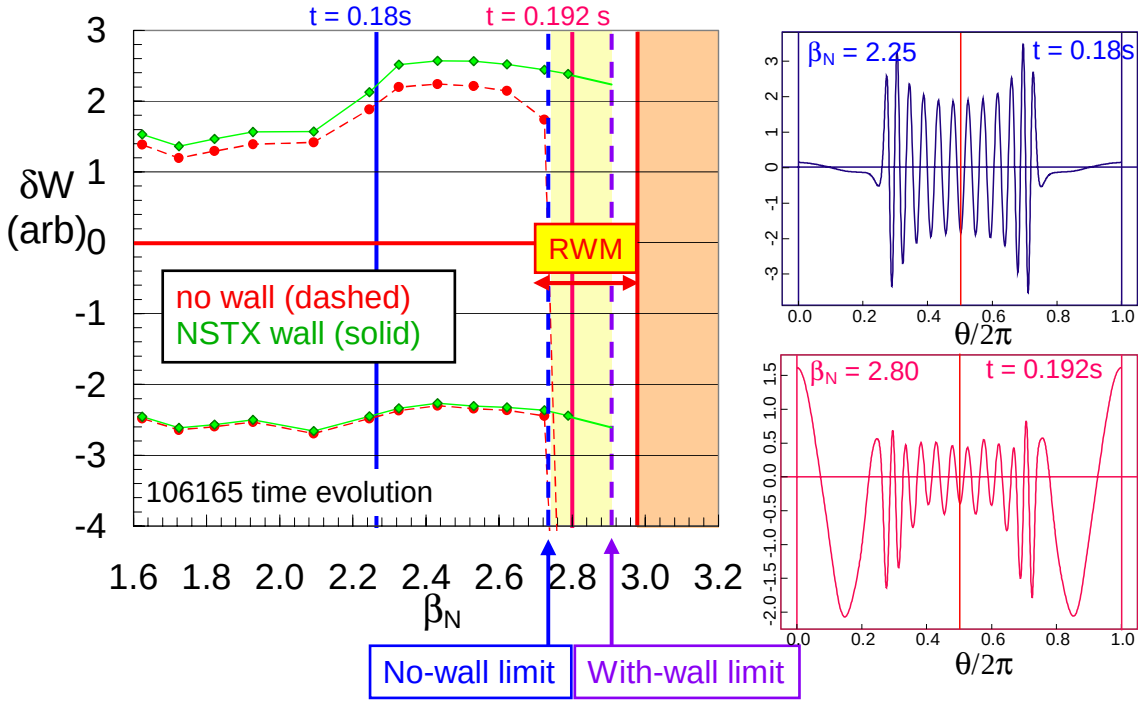
t = 0.18s
t = 0.192 s
δW (arb)
RWM
no wall (dashed)
NSTX wall (solid)
106165 time evolution
βN
No-wall limit
With-wall limit
βN = 2.25
t = 0.18s
θ/2π
βN = 2.80
t = 0.192s
θ/2π

FIG 11.

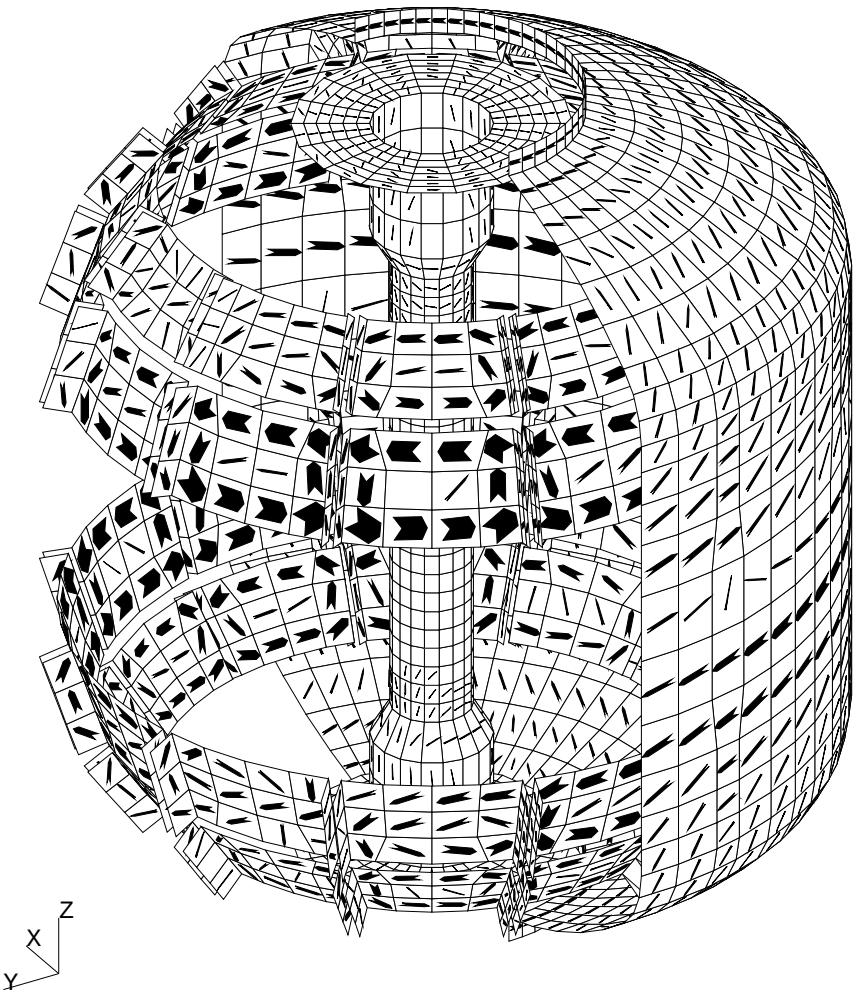

FIG 12.

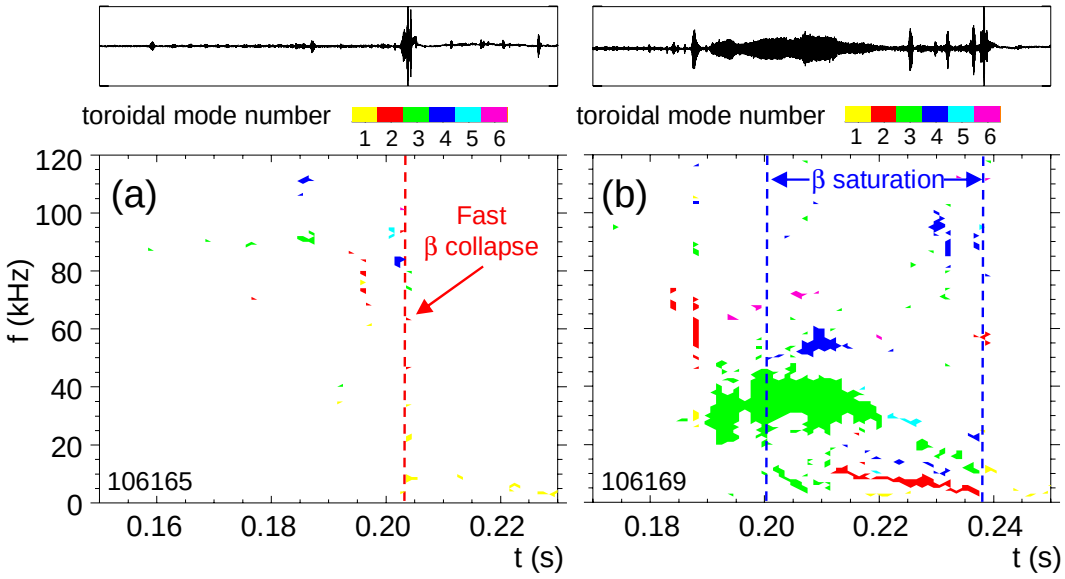
toroidal mode number
1 2 3 4 5 6
toroidal mode number
1 2 3 4 5 6
(a)
Fast
β collapse
106165
(b)
β saturation
106169
f (kHz)
120
100
80
60
40
20
0
0.16
0.18
0.20
0.22
t (s)
0.18
0.20
0.22
0.24
t (s)

FIG 13.

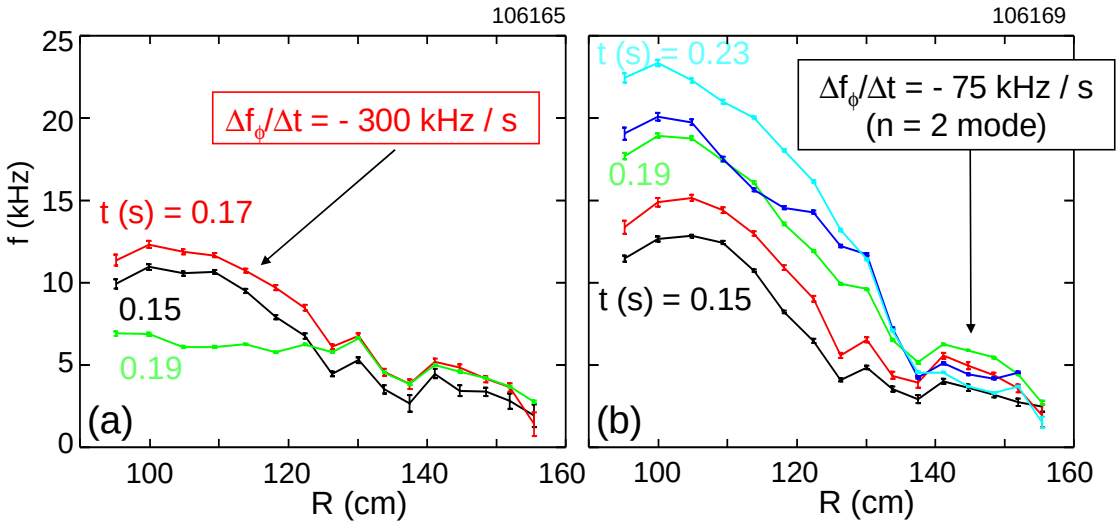
106165
106169
f (kHz)
R (cm)
R (cm)
Δf$_\phi$/Δt = - 300 kHz / s
t (s) = 0.17
0.15
0.19
(a)
t (s) = 0.23
0.19
t (s) = 0.15
Δf$_\phi$/Δt = - 75 kHz / s
(n = 2 mode)
(b)

FIG 14.

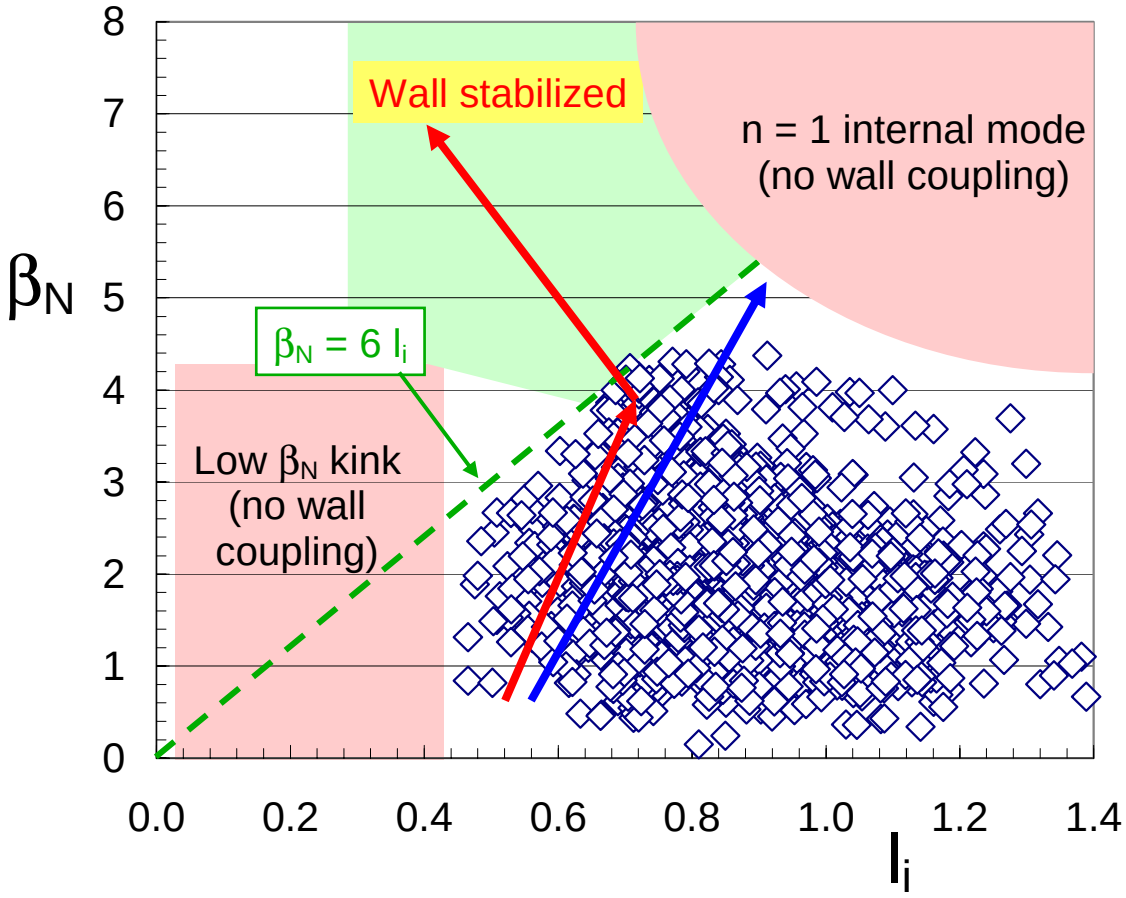
Wall stabilized
n = 1 internal mode
(no wall coupling)
$\beta_N = 6\, l_i$
Low β_N kink
(no wall
coupling)
β_N
l_i
0
1
2
3
4
5
6
7
8
0.0
0.2
0.4
0.6
0.8
1.0
1.2
1.4